Supporting Information

Highly conductive n-type $CH_3NH_3PbI_3$ single crystals doped with bismuth donors

Chen Li[a], Xin Chen[b], Ning Li[a], Jialiang Liu[a], Beilei Yuan[a], Yujiao Li,[b] Mei Wang[b], Yangqing Wu[b], Bingqiang Cao[a,b,*]

[a] Materials Research Center for Energy and Photoelectrochemical Conversion, School of Material Science and Engineering, University of Jinan, Jinan, 250022, Shandong, China

[b] School of Physics and Physical Engineering, Shandong Provincial Key Laboratory of Laser Polarization and Information Technology, Qufu Normal University, Qufu, 273165, Shandong, China

*Email: mse_caobq@ujn.edu.cn

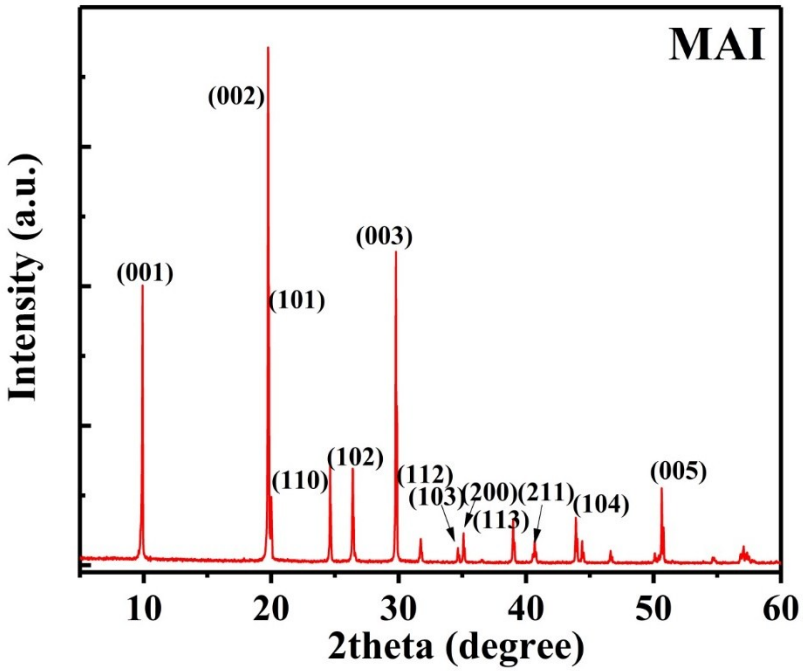

Figure S1. XRD pattern of synthesized CH_3NH_3I powder.

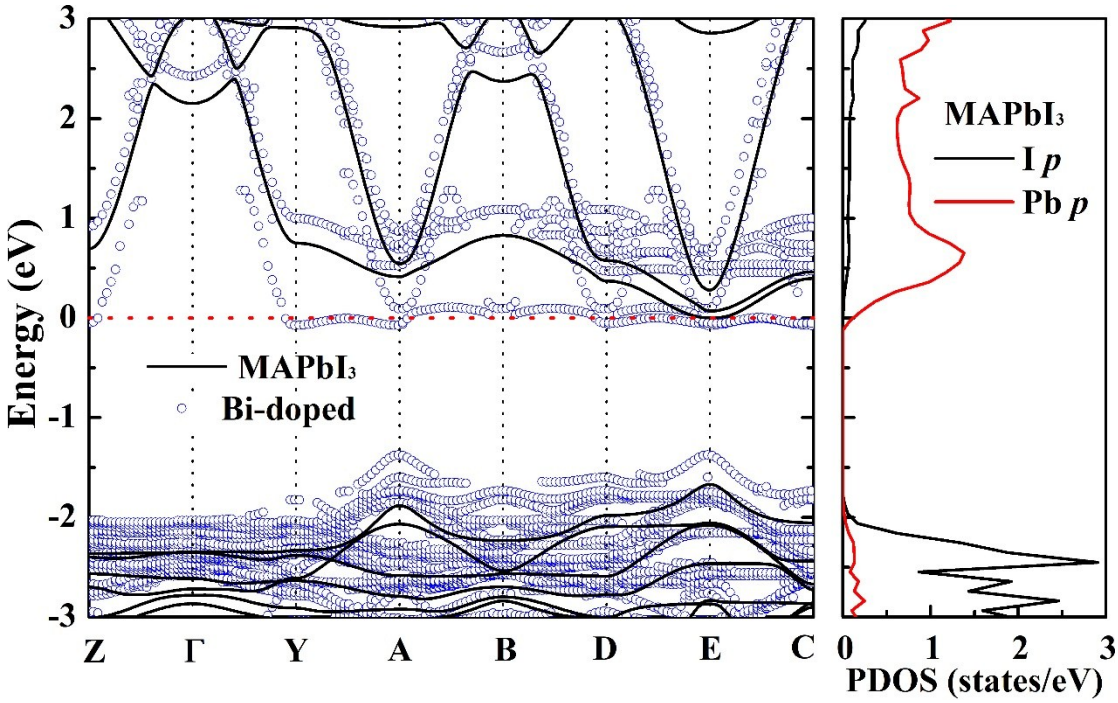

Figure S2. Calculated band structures and partial density of states (PDOS) for pristine $MAPbI_3$. For a clear comparison with band dispersions of Bi doping (blue circled lines), we shift Fermi level of pristine crystal to the conduction band minimum as denoted by the red dashed line at zero energy.

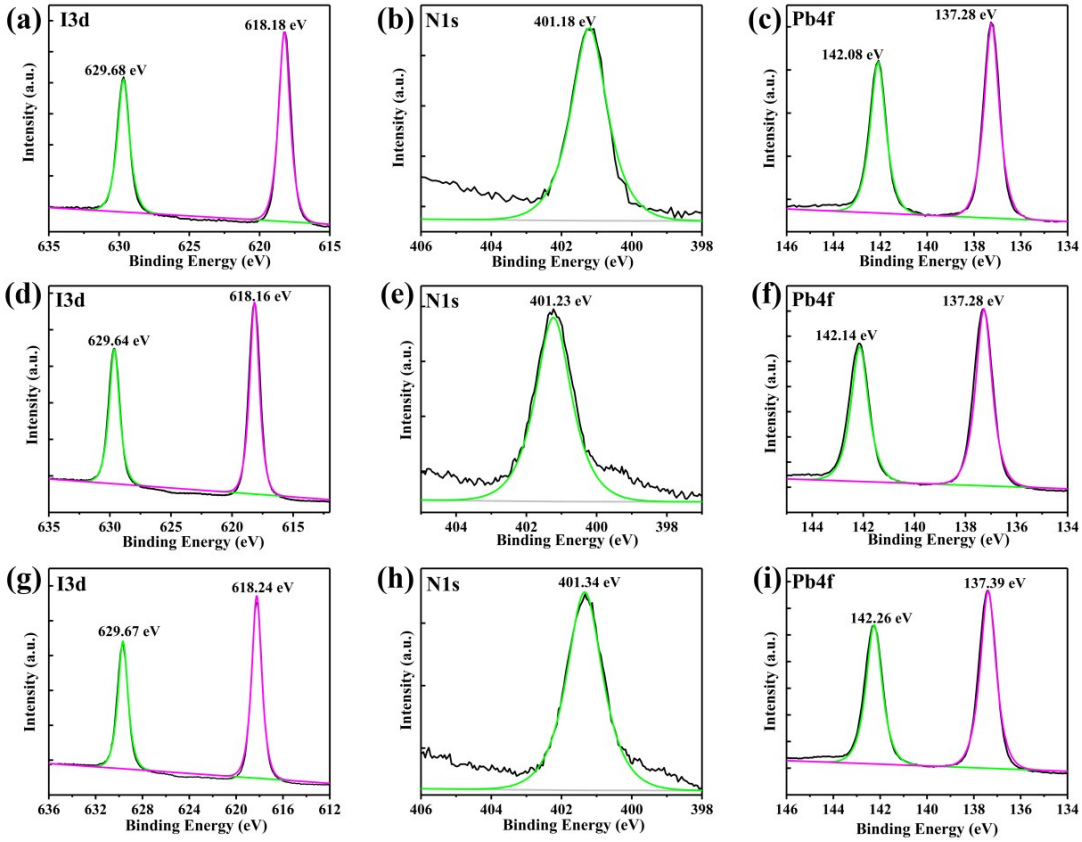

Figure S3. High-resolution XPS spectra of core level (a) I 3d, (b) N 1s, (c) Pb 4f in the un-doped $MAPbI_3$; High-resolution XPS spectra of core level (d) I 3d, (e) N 1s, (f) Pb 4f in the $MAPbI_3$ doped with 0.5% Bi^{3+}; High-resolution XPS spectra of core level (g) I 3d, (h) N 1s, (i) Pb 4f in the $MAPbI_3$ doped with 5% Bi^{3+}.

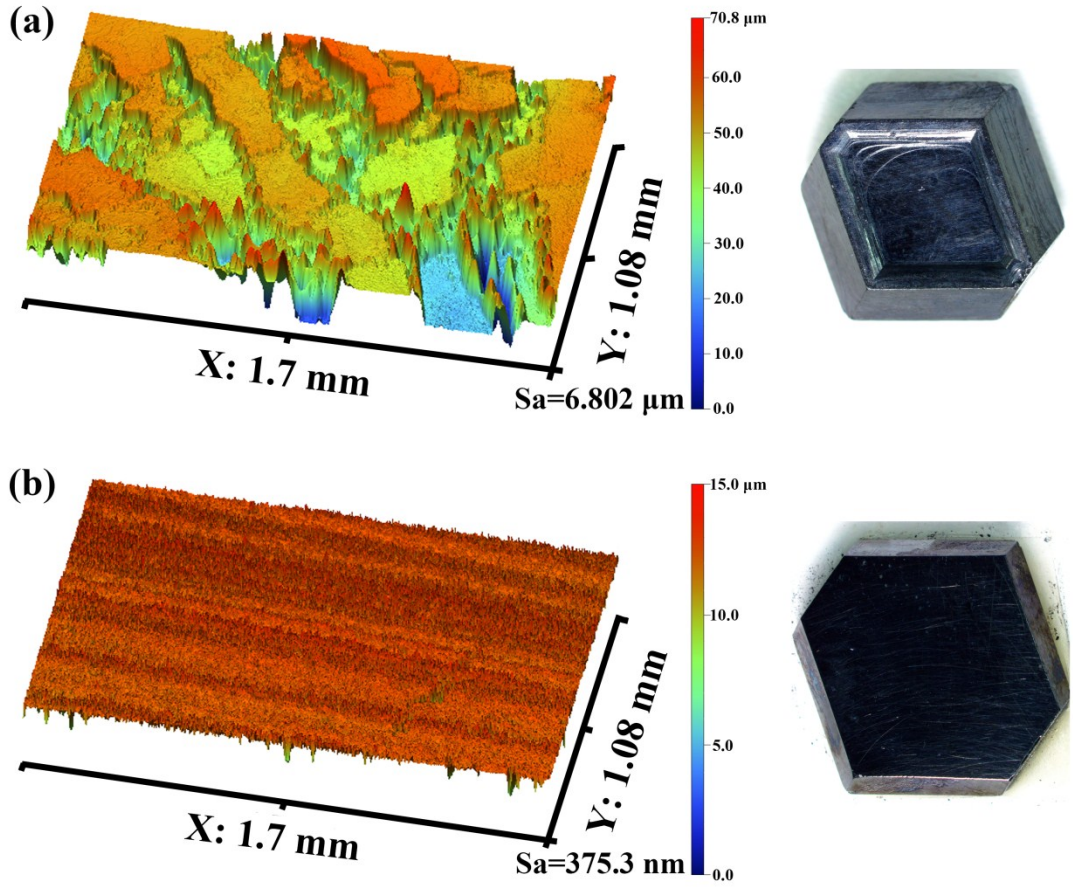

Figure S4. 3D profilometer images and surface topography photographs of (a) Un-polished (b) polished $MAPbI_3$ crystals; the average roughness is 6.802 µm and 375.3 nm, respectively.

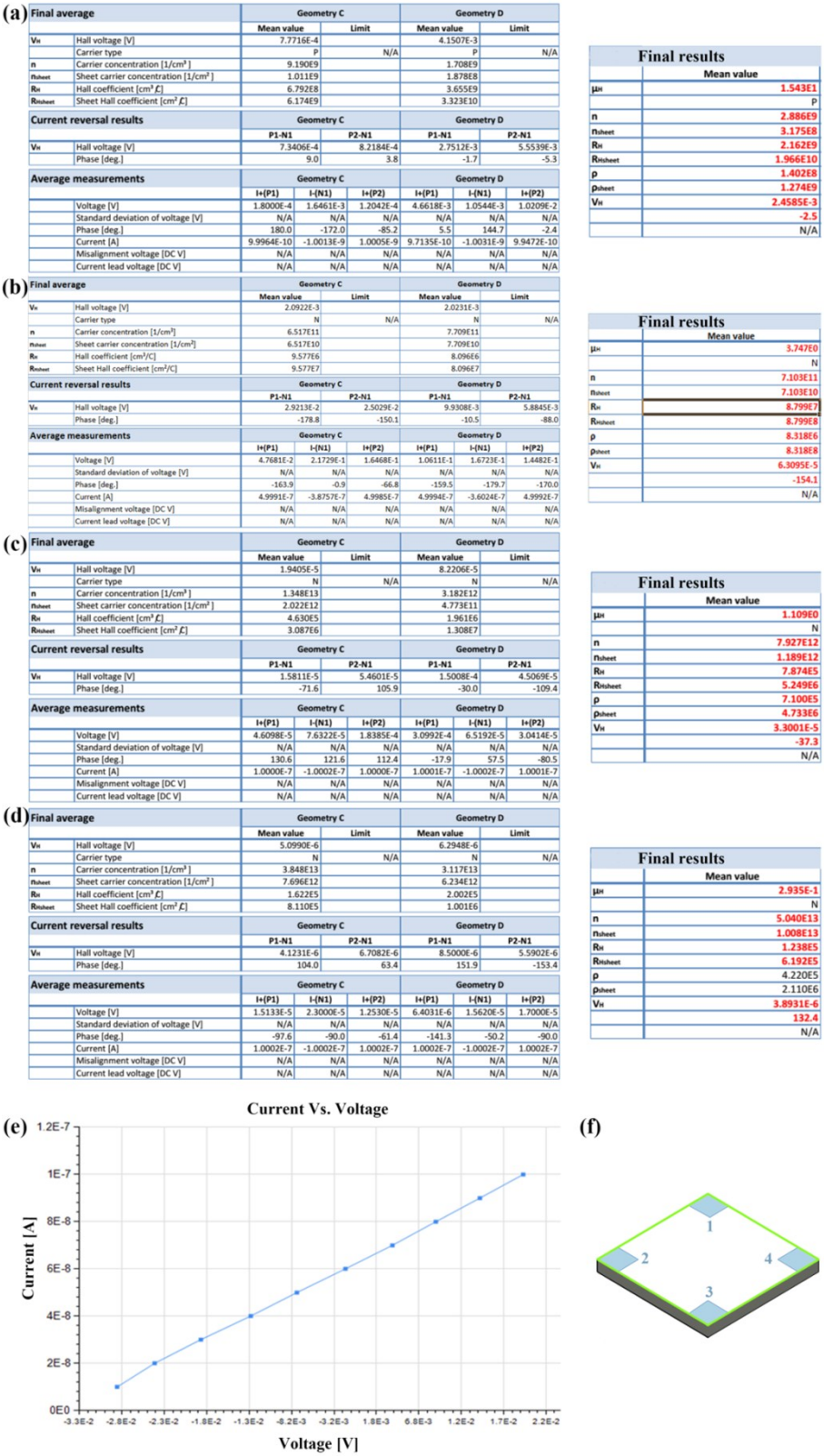

(a)

Final average		Geometry C		Geometry D	
		Mean value	Limit	Mean value	Limit
V_H	Hall voltage [V]	7.7716E-4		4.1507E-3	
	Carrier type	P	N/A	P	N/A
n	Carrier concentration [1/cm³]	9.190E9		1.708E9	
n_{sheet}	Sheet carrier concentration [1/cm²]	1.011E9		1.878E8	
R_H	Hall coefficient [cm³/C]	6.792E8		3.655E9	
R_{Hsheet}	Sheet Hall coefficient [cm²/C]	6.174E9		3.323E10	

Current reversal results		Geometry C		Geometry D	
		P1-N1	P2-N1	P1-N1	P2-N1
V_H	Hall voltage [V]	7.3406E-4	8.2184E-4	2.7512E-3	5.5539E-3
	Phase [deg.]	9.0	3.8	-1.7	-5.3

Average measurements		Geometry C			Geometry D		
		I+(P1)	I-(N1)	I+(P2)	I+(P1)	I-(N1)	I+(P2)
	Voltage [V]	1.8000E-4	1.6461E-3	1.2042E-4	4.6618E-3	1.0544E-3	1.0209E-2
	Standard deviation of voltage [V]	N/A	N/A	N/A	N/A	N/A	N/A
	Phase [deg.]	180.0	-172.0	-85.2	5.5	144.7	-2.4
	Current [A]	9.9964E-10	-1.0013E-9	1.0005E-9	9.7135E-10	-1.0031E-9	9.9472E-10
	Misalignment voltage [DC V]	N/A	N/A	N/A	N/A	N/A	N/A
	Current lead voltage [DC V]	N/A	N/A	N/A	N/A	N/A	N/A

Final results	Mean value
μ_H	1.543E1
	P
n	2.886E9
n_{sheet}	3.175E8
R_H	2.162E9
R_{Hsheet}	1.966E10
ρ	1.402E8
ρ_{sheet}	1.274E9
V_H	2.4585E-3
	-2.5
	N/A

(b)

Final average		Geometry C		Geometry D	
		Mean value	Limit	Mean value	Limit
V_H	Hall voltage [V]	2.0922E-3		2.0231E-3	
	Carrier type	N	N/A	N	N/A
n	Carrier concentration [1/cm³]	6.517E11		7.709E11	
n_{sheet}	Sheet carrier concentration [1/cm²]	6.517E10		7.709E10	
R_H	Hall coefficient [cm³/C]	9.577E6		8.096E6	
R_{Hsheet}	Sheet Hall coefficient [cm²/C]	9.577E7		8.096E7	

Current reversal results		Geometry C		Geometry D	
		P1-N1	P2-N1	P1-N1	P2-N1
V_H	Hall voltage [V]	2.9213E-2	2.5029E-2	9.9308E-3	5.8845E-3
	Phase [deg.]	-178.8	-150.1	-10.5	-88.0

Average measurements		Geometry C			Geometry D		
		I+(P1)	I-(N1)	I+(P2)	I+(P1)	I-(N1)	I+(P2)
	Voltage [V]	4.7681E-2	2.1729E-1	1.6468E-1	1.0611E-1	1.6723E-1	1.4482E-1
	Standard deviation of voltage [V]	N/A	N/A	N/A	N/A	N/A	N/A
	Phase [deg.]	-163.9	-0.9	-66.8	-159.5	-179.7	-170.0
	Current [A]	4.9991E-7	-3.8757E-7	4.9985E-7	4.9994E-7	-3.6024E-7	4.9992E-7
	Misalignment voltage [DC V]	N/A	N/A	N/A	N/A	N/A	N/A
	Current lead voltage [DC V]	N/A	N/A	N/A	N/A	N/A	N/A

Final results	Mean value
μ_H	3.747E0
	N
n	7.103E11
n_{sheet}	7.103E10
R_H	8.799E7
R_{Hsheet}	8.799E8
ρ	8.318E6
ρ_{sheet}	8.318E8
V_H	6.3095E-5
	-154.1
	N/A

(c)

Final average		Geometry C		Geometry D	
		Mean value	Limit	Mean value	Limit
V_H	Hall voltage [V]	1.9405E-5		8.2206E-5	
	Carrier type	N	N/A	N	N/A
n	Carrier concentration [1/cm³]	1.348E13		3.182E12	
n_{sheet}	Sheet carrier concentration [1/cm²]	2.022E12		4.773E11	
R_H	Hall coefficient [cm³/C]	4.630E5		1.961E6	
R_{Hsheet}	Sheet Hall coefficient [cm²/C]	3.087E6		1.308E7	

Current reversal results		Geometry C		Geometry D	
		P1-N1	P2-N1	P1-N1	P2-N1
V_H	Hall voltage [V]	1.5811E-5	5.4601E-5	1.5008E-4	4.5069E-5
	Phase [deg.]	-71.6	105.9	-30.0	-109.4

Average measurements		Geometry C			Geometry D		
		I+(P1)	I-(N1)	I+(P2)	I+(P1)	I-(N1)	I+(P2)
	Voltage [V]	4.6098E-5	7.6322E-5	1.8385E-4	3.0992E-4	6.5192E-5	3.0414E-5
	Standard deviation of voltage [V]	N/A	N/A	N/A	N/A	N/A	N/A
	Phase [deg.]	130.6	121.6	112.4	-17.9	57.5	-80.5
	Current [A]	1.0000E-7	-1.0002E-7	1.0000E-7	1.0001E-7	-1.0002E-7	1.0001E-7
	Misalignment voltage [DC V]	N/A	N/A	N/A	N/A	N/A	N/A
	Current lead voltage [DC V]	N/A	N/A	N/A	N/A	N/A	N/A

Final results	Mean value
μ_H	1.109E0
	N
n	7.927E12
n_{sheet}	1.189E12
R_H	7.874E5
R_{Hsheet}	5.249E6
ρ	7.100E5
ρ_{sheet}	4.733E6
V_H	3.3001E-5
	-37.3
	N/A

(d)

Final average		Geometry C		Geometry D	
		Mean value	Limit	Mean value	Limit
V_H	Hall voltage [V]	5.0990E-6		6.2948E-6	
	Carrier type	N	N/A	N	N/A
n	Carrier concentration [1/cm³]	3.848E13		3.117E13	
n_{sheet}	Sheet carrier concentration [1/cm²]	7.696E12		6.234E12	
R_H	Hall coefficient [cm³/C]	1.622E5		2.002E5	
R_{Hsheet}	Sheet Hall coefficient [cm²/C]	8.110E5		1.001E6	

Current reversal results		Geometry C		Geometry D	
		P1-N1	P2-N1	P1-N1	P2-N1
V_H	Hall voltage [V]	4.1231E-6	6.7082E-6	8.5000E-6	5.5902E-6
	Phase [deg.]	104.0	63.4	151.9	-153.4

Average measurements		Geometry C			Geometry D		
		I+(P1)	I-(N1)	I+(P2)	I+(P1)	I-(N1)	I+(P2)
	Voltage [V]	1.5133E-5	2.3000E-5	1.2530E-5	6.4031E-6	1.5620E-5	1.7000E-5
	Standard deviation of voltage [V]	N/A	N/A	N/A	N/A	N/A	N/A
	Phase [deg.]	-97.6	-90.0	-61.4	-141.3	-50.2	-90.0
	Current [A]	1.0002E-7	-1.0002E-7	1.0002E-7	1.0002E-7	-1.0002E-7	1.0002E-7
	Misalignment voltage [DC V]	N/A	N/A	N/A	N/A	N/A	N/A
	Current lead voltage [DC V]	N/A	N/A	N/A	N/A	N/A	N/A

Final results	Mean value
μ_H	2.935E-1
	N
n	5.040E13
n_{sheet}	1.008E13
R_H	1.238E5
R_{Hsheet}	6.192E5
ρ	4.220E5
ρ_{sheet}	2.110E6
V_H	3.8931E-6
	132.4
	N/A

(e)

(f)

Figure S5. Original log sheet of the Hall Effect measurement for (a) Un-doped, (d) 1% Bi^{3+} (c) 5% Bi^{3+} and (d) 10% Bi^{3+} doped $MAPbI_3$. (e) The current-voltage properties to be used for contact check. (f) The contact configuration used in Hall Effect measurements (the blue corners are the contacts).

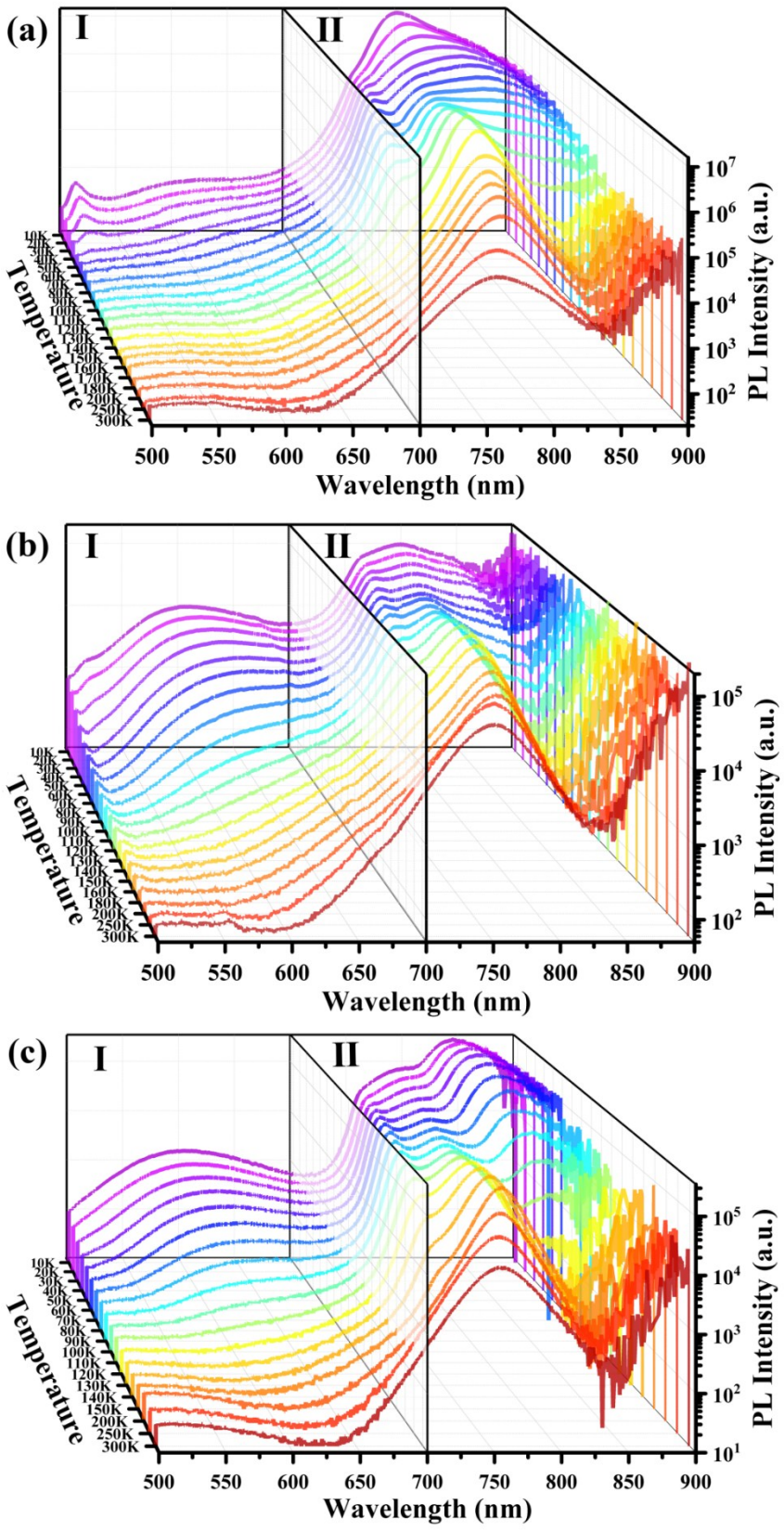

Figure S6.Temperature-dependent PL spectra of (a) Un-doped, (b) 5% Bi^{3+} and (c) 10% Bi^{3+} doped $MAPbI_3$ for temperatures in the 10-300 K.

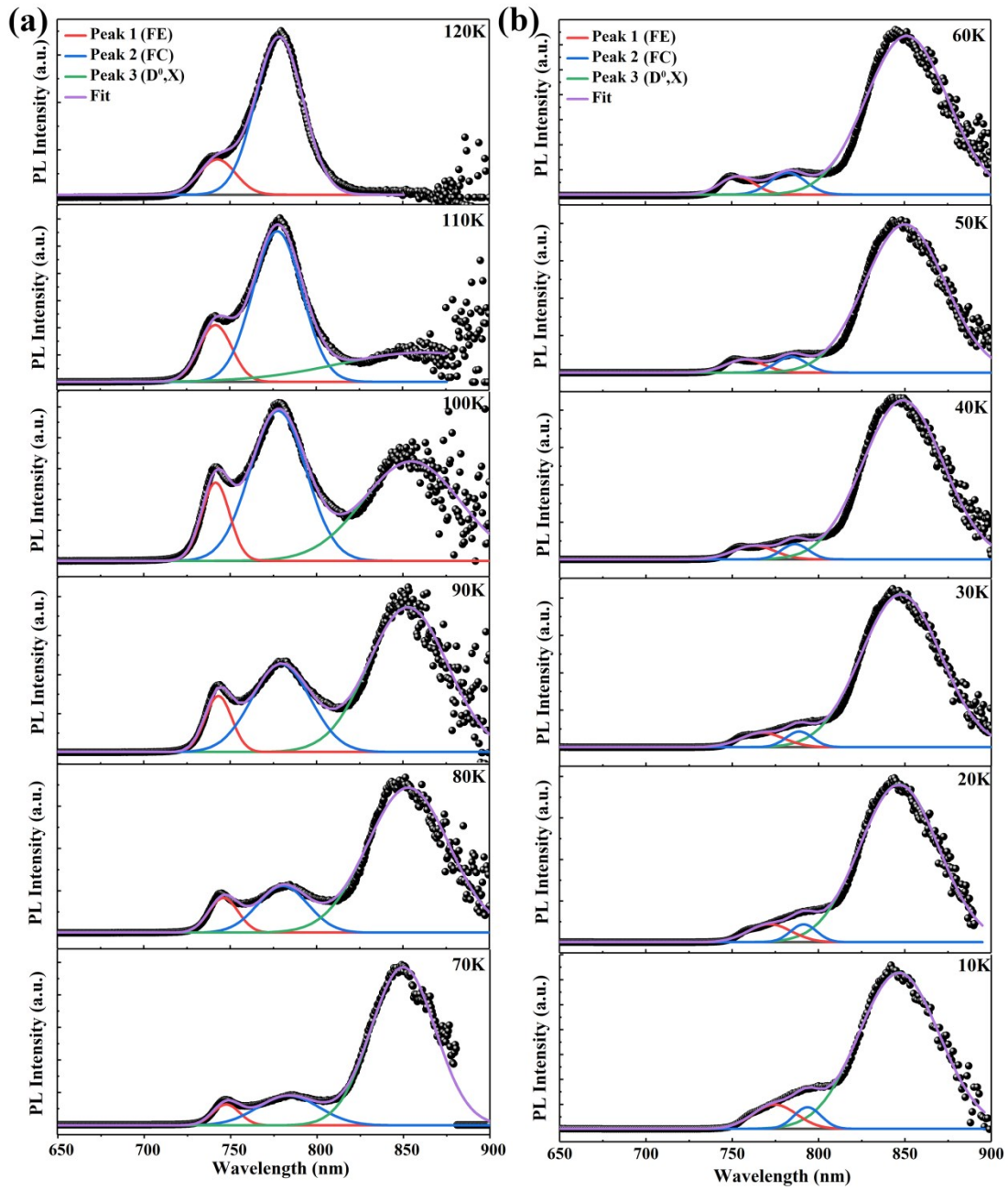

Figure S7. Typical Gaussian-fitting analysis of the PL spectrum, for temperatures in the 10-120 K range ((a) (b)).

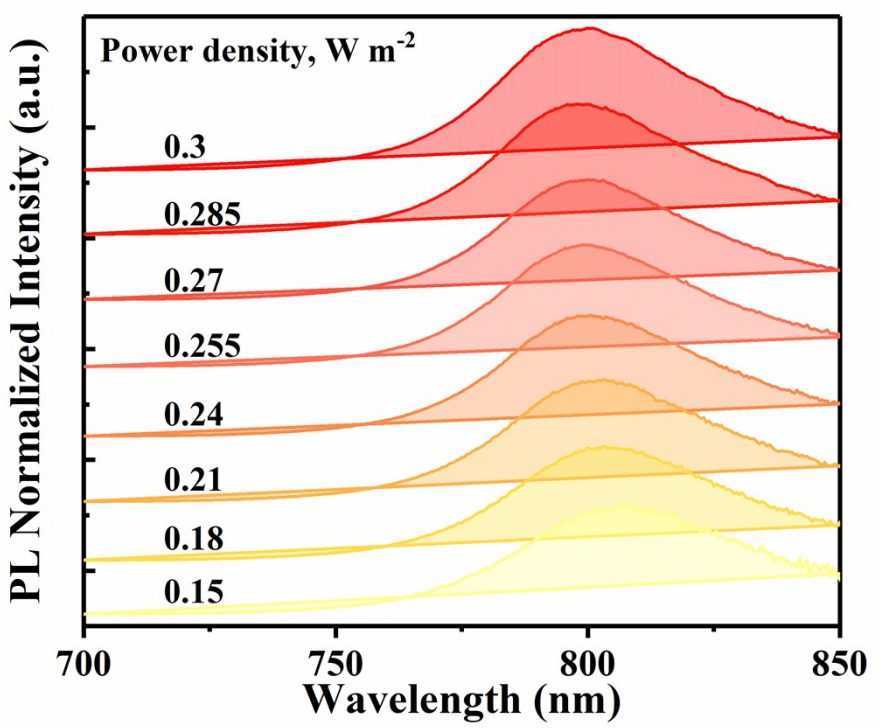

Figure S8. The un-doped crystals PL normalized spectra at 10 K measured at different power densities.

Table S1. Decay parameters and average lifetime according to a double exponential functions fitting model of the PL decay curves obtained from the samples.

Sample	τ_1 (µs)	τ_2 (µs)	R^2
0% Bi	14.1	0.36	0.96
0.5% Bi	10.9	1.11	0.99
1% Bi	7.7	0.49	0.99
5% Bi	4.29	0.26	0.96
10% Bi	3.73	0.59	0.99

Supporting Note 1:

When the temperature is further below 150 K, Peak II exhibits blueshift and then redshift behavior. This behavior can be understood within the Bose-Einstein model[1],

$$E_{A2}(T) - E_{A2}^{0} = \frac{\partial E_{A2}(T)}{\partial V}\frac{\partial V}{\partial T}T + A_{EP}\left[\frac{2}{(exp(\hbar\omega/kT) - 1)} + 1\right] \qquad (1)$$

The first term in this equation describes the change in the band gap associated with the thermal expansion of the lattice. As the $\frac{\partial V}{\partial T}$ of $MAPbI_3$ is positive, the band gap increases with increasing lattice constant.[2, 3] The second term accounts for the band gap renormalization due to the electron-phonon coupling, where A_{EP} is the strength of the coupling. A_{EP} is typically negative and give rise to an increase in band gap with the decrease of temperature.[4] In the temperature range of 150 K-110 K, the electron-phonon coupling plays a major role, and the abnormal phenomena that the bandgap increase with the decrease of temperature occurs. When the temperature continues to reduce from 110 K to 10 K, the lattice vibrations is suppressed, and the phonon number is reduced. Hence, the peak redshift (18 nm) originates from the band gap narrowing caused by the lattice contraction.

SUPPORTING REFERENCES:

1. Lautenschlager, Garriga, Logothetidis and Cardona, *Phy. Rev. B, Condens. Matter*, 1987, **35**, 9174-9189.

2. M. I. Dar, G. Jacopin, S. Meloni, A. Mattoni, N. Arora, A. Boziki, S. M. Zakeeruddin, U. Rothlisberger and M. Gratzel, *Sci. Adv*., 2016, **2**, 9.

3. S. Meloni, G. Palermo, N. Ashari-Astani, M. Gratzel and U. Rothlisberger, *J. Mater. Chem. A*, 2016, **4**, 15997-16002.

4. K. Wei, Z. J. Xu, R. Z. Chen, X. Zheng, X. G. Cheng and T. Jiang, *Opt. Lett.*, 2016, **41**, 3821-3824.